LETTER

doi:10.1038/nature10665

Predicting mutation outcome from early stochastic variation in genetic interaction partners

Alejandro Burga[1], M. Olivia Casanueva[1] & Ben Lehner[1,2]

Many mutations, including those that cause disease, only have a detrimental effect in a subset of individuals. The reasons for this are usually unknown, but may include additional genetic variation and environmental risk factors[1]. However, phenotypic discordance remains even in the absence of genetic variation, for example between monozygotic twins[2], and incomplete penetrance of mutations is frequent in isogenic model organisms in homogeneous environments[3,4]. Here we propose a model for incomplete penetrance based on genetic interaction networks[5,6]. Using *Caenorhabditis elegans* as a model system, we identify two compensation mechanisms that vary among individuals and influence mutation outcome. First, feedback induction of an ancestral gene duplicate differs across individuals, with high expression masking the effects of a mutation. This supports the hypothesis that redundancy is maintained in genomes to buffer stochastic developmental failure[7]. Second, during normal embryonic development we find that there is substantial variation in the induction of molecular chaperones such as Hsp90 (DAF-21). Chaperones act as promiscuous buffers of genetic variation[8,9], and embryos with stronger induction of Hsp90 are less likely to be affected by an inherited mutation. Simultaneously quantifying the variation in these two independent responses allows the phenotypic outcome of a mutation to be more accurately predicted in individuals. Our model and methodology provide a framework for dissecting the causes of incomplete penetrance. Further, the results establish that inter-individual variation in both specific and more general buffering systems combine to determine the outcome inherited mutations in each individual.

It is well established that isogenic individuals show substantial variation at the molecular level, for example in the expression levels of particular genes[10]. This variation can be an important influence on signalling and development in wild-type (WT) individuals[11,12]. Such molecular variation may also influence the phenotypic consequences of inherited mutations, but examples of molecular variation have only been described that predict phenotypic variation at the level of other molecules[13] or cellular phenotypes[14].

To identify determinants of mutation outcome, we present a model for incomplete penetrance based on genetic interaction networks[5,6] (Fig. 1b). Our model proposes that in the absence of additional genetic variation, it is stochastic variation in the abundance or activity of genetic interaction partners (genes that influence the outcome of a mutation when genetically altered) that determines the outcome of a mutation (Fig. 1d). The correlated loss of genetic, environmental and stochastic robustness upon gene deletion in yeast is highly consistent with the generality of this proposal[6,15].

To test our model, we first used a null mutation in the T-box transcription factor gene *tbx-9* (Supplementary Fig. 1) that causes an incompletely penetrant defect in *C. elegans* larval morphology owing to abnormal development of the epidermis and muscle[16,17] (Fig. 1a). Transcription factor *tbx-9* is related to another transcription factor, *tbx-8*, by an ancestral gene duplication; inactivation of *tbx-8* causes similar incompletely penetrant defects, and loss of both genes results in synthetic lethality in *C. elegans*[16,17] and *Caenorhabditis briggsae*[18].

If the incomplete penetrance of *tbx-9* relates to variation in the expression of *tbx-8*, then increased expression of *txb-8* should be able to compensate for the loss of *tbx-9*. Expression of TBX-8 from a transgene indeed reduces the penetrance of a *tbx-9*(*ok2473*) null allele (Fig. 1c and Supplementary Fig. 2). A further requisite of our model is the existence of inter-individual variation in the expression of the genetic interaction partner. We quantified the induction of a fluorescent reporter driven by the *tbx-8* promoter (*ptbx-8::GFP*) during normal development and found that there was substantial variation among embryos (Fig. 2a) with an important extrinsic component (Supplementary Figs 3a and 4).

We next quantified the induction of the *tbx-8* reporter in *tbx-9*(*ok2473*) mutant animals and found that expression was increased (Fig. 2b, 1.2-fold upregulation at comma stage, $P = 1.6 \times 10^{-3}$). We confirmed this upregulation by performing single molecule fluorescence *in situ* hybridization against the endogenous *tbx-8* messenger RNA (mRNA) (Supplementary Fig. 5, 1.6-fold upregulation in 40- to

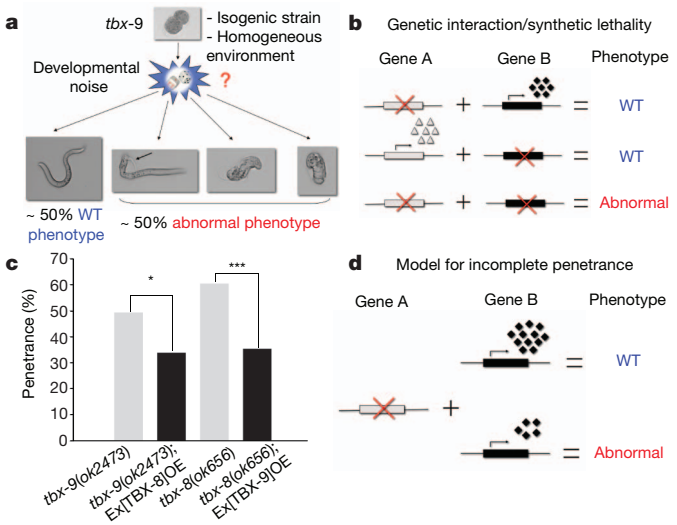

Figure 1 | Genetic interactions provide a general model for incomplete penetrance. **a**, Inactivation of the gene *tbx-9* in *C. elegans* results in an incompletely penetrant defect, with approximately half of embryos hatching with abnormal morphology (small arrow). **b**, Representation of a negative (synergistic) genetic interaction between two genes *A* and *B*. **c**, Increased expression of TBX-8 reduces the penetrance of a *tbx-9*(*ok2473*) null mutation (49% ($n = 138$) compared with 34% ($n = 139$), a 33% decrease in abnormal phenotypes, $P = 0.011$, Fisher's exact test). Likewise, increased TBX-9 expression rescues the penetrance of a *tbx-8*(*ok656*) null mutation (60% ($n = 164$) compared with 35% ($n = 195$), a 42% decrease, $P = 2.8 \times 10^{-6}$). **d**, A model for incomplete penetrance based on variation in the activity of genetic interaction partners.

[1]EMBL-CRG Systems Biology Unit, Centre for Genomic Regulation (CRG) and Universitat Pompeu Fabra (UPF), Barcelona 08003, Spain. [2]Institució Catalana de Recerca i Estudis Avançats, Centre for Genomic Regulation (CRG) and Universitat Pompeu Fabra (UPF), Barcelona 08003, Spain.

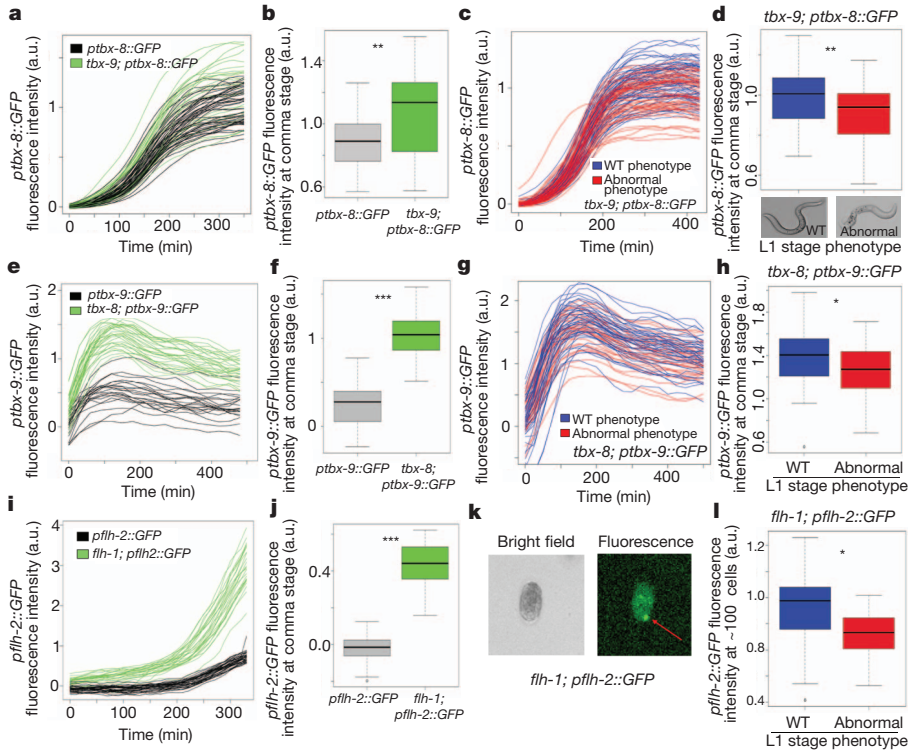

Figure 2 | Early inter-individual variation in the induction of ancestral gene duplicates predicts the outcome of inherited mutations. **a**, Quantification of total green fluorescent protein (GFP) expression from a *tbx-8* reporter during embryonic development in WT (black) and *tbx-9*(*ok2473*) (green) individuals. Each individual is a separate line. a.u., Arbitrary units. **b**, Boxplot of *tbx-8* reporter expression (**a**) showing 1.2-fold upregulation in a *tbx-9* mutant at comma stage (~290 min, $P = 1.6 \times 10^{-3}$, Wilcoxon rank test). **c**, Expression of *tbx-8* reporter in a *tbx-9*(*ok2473*) background for embryos that hatch with (red) or without (blue, WT) a morphological defect. **d**, Boxplot of **c** showing *tbx-8* expression is higher in *tbx-9* embryos that develop a WT phenotype (blue) compared with those that develop an abnormal (red) phenotype at comma stage ($P = 6.1 \times 10^{-3}$). **e**, Expression of a *ptbx-9::GFP* reporter in WT (black) and *tbx-8*(*ok656*) mutant (green). **f**, Boxplot of *tbx-9* reporter showing 4.3-fold upregulation at comma stage (~375 min, $P = 3.6 \times 10^{-16}$). **g**, Expression of *tbx-9* reporter in a *tbx-8*(*ok656*) mutant background, colour code as in **c**. **h**, Boxplot of **g** showing *tbx-9* expression is higher in *tbx-8* embryos that develop a WT phenotype ($P = 0.033$). **i**, Expression of a *pflh-2::GFP* reporter in WT (black) and *flh-1*(*bc374*) mutant (green). **j**, Boxplot of *flh-2* reporter expression (**i**) showing 1.8-fold upregulation in a *flh-1* mutant at comma stage (~180 min, $P = 2.2 \times 10^{-16}$). **k**, Bright-field and fluorescence image of an approximate 100-cell *flh-1*; *pflh-2::GFP* embryo. Red arrow indicates the local expression of *flh-2* reporter quantified for *flh-1* phenotypic prediction. **l**, Boxplot showing higher *flh-2* reporter expression at approximate 100 cells for WT (blue) compared with abnormal (red) phenotypes ($P = 0.014$). Boxplots show the median, quartiles, maximum and minimum expression in each data set.

50-cell-stage embryos, $P = 5.3 \times 10^{-4}$). Thus, a direct or indirect feedback mechanism exists that upregulates transcription of *tbx-8* when its ancestral paralogue is inactivated. This feedback also acts on the *tbx-9* promoter, which is also upregulated in a *tbx-9*(*ok2473*) mutant background (Supplementary Fig. 6). This is highly consistent with observations that have been made in yeast[19,20] and suggests that compensatory expression by negative feedback regulation of gene duplicates is probably a conserved phenomenon across species.

Next, we tested whether variation in the induction of *tbx-8* correlated with the outcome of the *tbx-9*(*ok2473*) mutation at hatching. We retrospectively compared the early expression of the reporter in embryos that did, and did not, hatch with an abnormal phenotype. Early expression was higher in the second class (Fig. 2c, d, $P = 6.1 \times 10^{-3}$); whereas 80% of the embryos with reporter expression in the highest quartile hatched without a defect, only 40% of those in the lowest quartile showed no phenotype (Supplementary Table 1, $P = 3.3 \times 10^{-3}$). In contrast, early expression from a ubiquitously transcribed promoter (*plet-858::GFP*) did not predict phenotypic outcome in individuals (Supplementary Fig. 7a, b, $P = 0.58$), nor did variation in the expression of a reporter for the transcription factor ELT-5, another protein required for epidermal development[21] (Supplementary Fig. 7c, d, $P = 0.97$). High expression of the synthetic lethal partner *tbx-8*, but not high transcription in general, is therefore partly epistatic[22] to the loss of *tbx-9*. We also tested the reverse situation: that is, whether variation in *tbx-9* expression compensation (Fig. 2e, f, 4.3-fold upregulation, $P = 3.6 \times 10^{-16}$) predicted the phenotypic outcome of a *tbx-8*(*ok656*) mutation. We found that was indeed the case (Fig. 2g, h, $P = 0.033$, see Supplementary Table 1).

The FLYWCH transcription factors *flh-1* and *flh-2* are an additional pair of ancestral gene duplicates that redundantly repress embryonic expression of the microRNAs *lin-4*, *mir-48* and *mir-241* (ref. 23). Similar to the case for *tbx-9* null mutants, *flh-1*(*bc374*) mutant embryos induced higher levels of a *pflh-2::GFP* reporter than WT embryos (Fig. 2i, j, 1.8-fold at comma stage, $P < 2.2 \times 10^{-16}$). In contrast, we found neither upregulation of a *tbx-8* reporter in an *flh-1*(*bc374*) background, nor upregulation of an *flh-2* reporter in a *tbx-9*(*ok2473*) mutant (Supplementary Fig. 8, $P = 0.74$ and $P = 0.55$ respectively). *flh-1*(*bc374*) embryos that expressed higher *flh-2* reporter levels early in development (Fig. 2k, see Methods) were, however, more likely to develop into morphologically WT larvae (Fig. 2l, $P = 0.014$, see Supplementary Table 1). In contrast, we found that *pflh-2::GFP* reporter levels did not predict the outcome of a *tbx-9*(*ok2473*) null mutation (Supplementary Fig. 7g, h, $P = 0.32$), nor did induction of the *ptbx-8::GFP* reporter predict the outcome of the *flh-1*(*bc374*) mutation (Supplementary Fig. 7e, f, $P = 0.49$).

Many ancestral gene duplicates have retained partly redundant functions over extensive evolutionary periods[19,24,25]. One explanation for this could be the selection pressure provided by stochastic developmental errors[7,26] ('canalization'[27]). Our results provide direct empirical support for this hypothesis, showing that when one member of a partly

redundant gene pair is inactivated, expression variation in the other gene becomes an important influence on the phenotype of an individual.

The variation in the induction *tbx-8* that we can quantify only partly accounts for variation in the outcome of the *tbx-9* mutation (Fig. 2d). We considered that one additional influence on mutation outcome could be variation in the activity of general buffering systems such as molecular chaperones. In multiple eukaryotes, chaperone inhibition can enhance the effects of diverse mutations[8,9,28] and increased chaperone activity promiscuously suppresses detrimental mutations in bacteria[29,30].

We constructed a transcriptional reporter for the constitutively expressed chaperone *daf-21* (*Hsp90*). Variability in the *pdaf-21::mCherry* reporter was evident during all larval stages and, surprisingly, its induction during embryonic development also varied substantially, even in the absence of a mutation or environmental perturbation (Supplementary Figs 9a and 10). No difference in transgene copy number was detected between animals with high or low *daf-21* reporter expression (Supplementary Fig. 11), and individuals with high reporter expression have high expression of the DAF-21 protein (Fig. 3a and Supplementary Fig. 12).

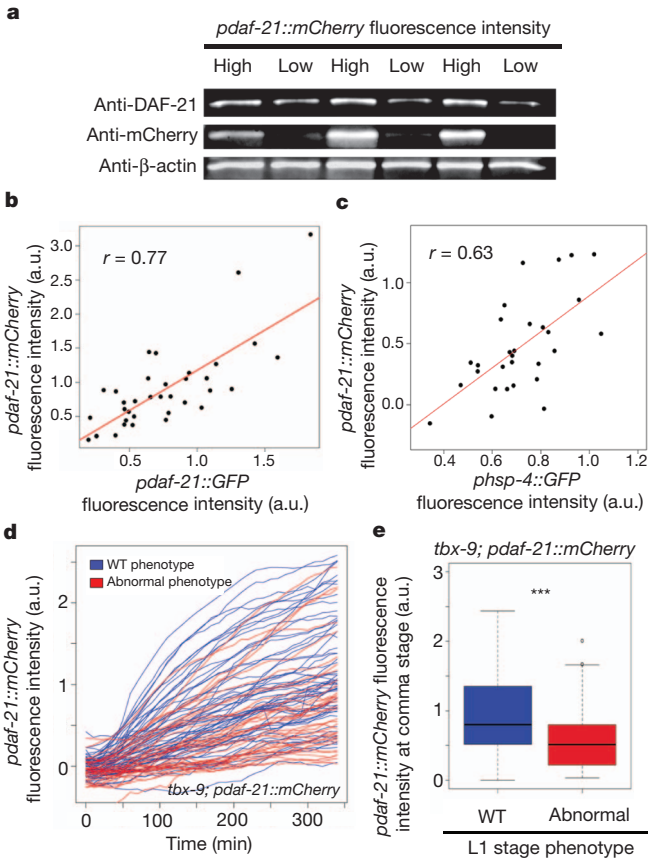

Figure 3 | Inter-individual variation in chaperone induction predicts the outcome of a mutation. **a**, *pdaf-21::mCherry; glp-1(e2141)* animals were sorted into 'high' and 'low' groups based on their *pdaf-21::mCherry* expression 24 h after the L1 stage at 25 °C. Western blot analysis confirmed that worms belonging to the 'high' group had higher levels of endogenous DAF-21 protein. As a positive control, mCherry protein levels showed the same trend. β-Actin was used as loading control; results of three replica sortings are shown. **b**, **c**, Correlation in individuals (measured at comma stage) between: *pdaf-21::mCherry* and *pdaf-21::GFP* (Pearson correlation coefficient, $r = 0.77$, $P = 3.4 \times 10^{-8}$) (**b**); *pdaf-21::mCherry* and *phsp-4::GFP* ($r = 0.63$, $P = 2.8 \times 10^{-4}$) (**c**). **d**, **e**, Expression of *daf-21* reporter in a *tbx-9(ok2473)* mutant background. Embryos that hatch into phenotypically WT worms (blue) have higher expression than those hatching with a morphological defect (red) at the comma stage ($P = 1.9 \times 10^{-3}$).

We tested whether this variability was particular to *daf-21* or common to other chaperones using a reporter for the gene *hsp-4* (orthologous to mammalian BiP). Transcription from the *hsp-4* promoter also varied extensively among embryos (Supplementary Fig. 13) and was correlated with that from the *daf-21* promoter (Fig. 3c, Pearson correlation coefficient, $r = 0.63$, $P = 2.8 \times 10^{-4}$), similar to the correlation between two independent *daf-21* reporters (Fig. 3b, $r = 0.77$, $P = 3.4 \times 10^{-4}$). This and additional correlations between stress response genes (Supplementary Fig. 14) suggest that, during normal development, isogenic embryos differ in a coordinated manner in the transcriptional induction of multiple chaperones.

We quantified induction of a *pdaf-21::mCherry* reporter in a *tbx-9(ok2473)* background. The mean induction of this reporter was increased in *tbx-9(ok2473)* animals (Supplementary Fig. 9b, 1.8-fold upregulation, $P = 6.6 \times 10^{-4}$). In addition, embryos that later hatched without a morphological defect expressed higher levels of the reporter

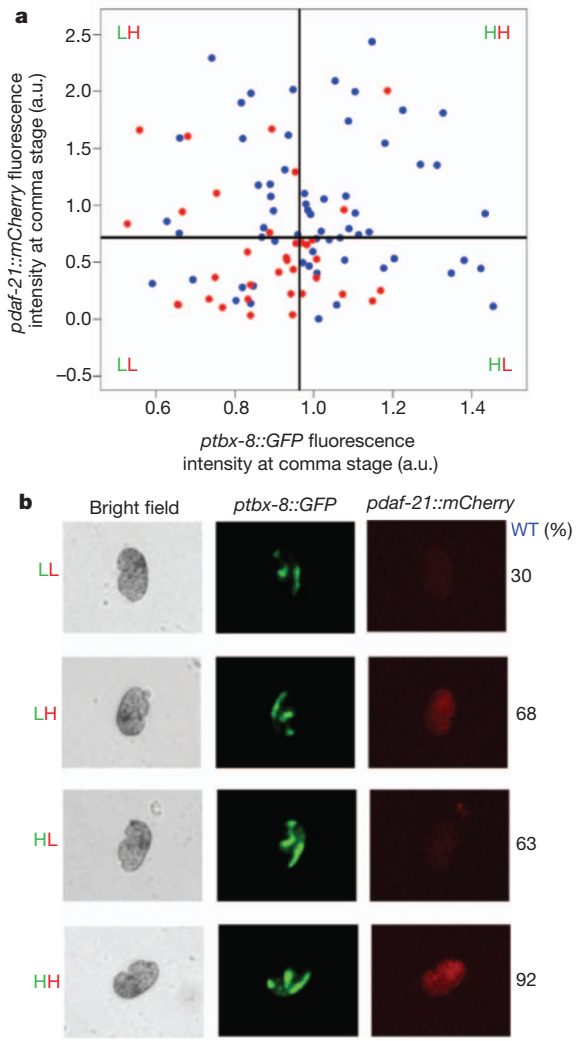

Figure 4 | Simultaneous quantification of inter-individual variation in two buffering systems accurately predicts the outcome of a mutation. **a**, Expression levels of *tbx-8* and *daf-21* reporters in individual *tbx-9(ok2473)* mutant embryos at the comma stage of development are not correlated ($r = 0.061$, $P = 0.56$). Each point represents one individual embryo. Embryos that hatched into phenotypically WT larvae are blue; embryos that hatched with a morphological defect are red. The median values for each reporter are indicated (black lines); embryos with expression above or below the median are defined as high (H) and low (L), respectively. **b**, Percentage of embryos from each expression class hatching with normal morphology. Representative bright-field, green and red fluorescence images are shown. Prediction scores for different time points and measures are given in Supplementary Table 3.

early on in development (Fig. 3d, e, $P = 1.9 \times 10^{-3}$, see Supplementary Table 1). The *daf-21* reporter also predicted *tbx-8*(*ok656*) mutation outcome (Supplementary Figs 15 and 16). Higher chaperone expression during early embryonic development therefore predicts a reduced effect of the inherited mutation.

We next constructed a strain allowing us to quantify simultaneously inter-individual variation in the expression of both buffering systems. Expression from the *tbx-8* and *daf-21* reporters does not correlate across individuals (Fig. 4a, $r = 0.061$, $P = 0.56$), showing that the two buffering systems vary independently. We retrospectively divided *tbx-9*(*ok2473*) mutation embryos into four approximately equally populated groups, depending upon whether their expression was above or below the median for each of the reporters, and examined the proportion of individuals hatching as WT larvae in each group (Fig. 4b). Whereas 30% of embryos with below-median expression of both reporters hatched without an abnormal phenotype ('LL' embryos, Fig. 4a, b, $P = 1.7 \times 10^{-5}$), 68% and 63% of embryos with above-median expression of a single reporter (*daf-21* or *tbx-8*, respectively) showed no morphological defect (Fig. 4b). Strikingly, 92% of embryos with above median expression of both reporters hatched as phenotypically WT larvae ('HH' embryos, Fig. 4a, b). That is, non-genetic variation in two buffering systems can be almost completely epistatic[22] to the *tbx-9* mutation. Receiver operating characteristic curve analysis confirmed the independent contribution of both reporters to phenotypic predictions (Supplementary Fig. 17).

In summary, we have shown here that incomplete penetrance is not just a direct consequence of failure caused by mutations[13,14], but that organisms have plastic compensatory responses[19] in both specific and more promiscuous genetic interaction partners that vary among individuals. It is the combination of this variation that determines the outcome of each mutation in each individual.

Inherited mutations also frequently have variable consequences in other species, including in human disease[2]. Based on our findings in *C. elegans*, we propose that incomplete genetic compensation may play a role in human disease, influencing the outcome of inherited polymorphisms in each individual.

METHODS SUMMARY

The expression from individual developing embryos was quantified using customized imaging and analysis protocols. Embryos were released from adult worms by dissection and sorted according to their developmental stage. Phenotypes were scored at hatching. Reporter constructs were generated by microinjection or bombardment.

Full Methods and any associated references are available in the online version of the paper at www.nature.com/nature.

Received 15 February; accepted 21 October 2011.

1. Badano, J. L. & Katsanis, N. Beyond Mendel: an evolving view of human genetic disease transmission. *Nature Rev. Genet.* **3,** 779–789 (2002).
2. Baranzini, S. E. *et al.* Genome, epigenome and RNA sequences of monozygotic twins discordant for multiple sclerosis. *Nature* **464,** 1351–1356 (2010).
3. Horvitz, H. R. & Sulston, J. E. Isolation and genetic characterization of cell-lineage mutants of the nematode *Caenorhabditis elegans*. *Genetics* **96,** 435–454 (1980).
4. Gartner, K. A third component causing random variability beside environment and genotype. A reason for the limited success of a 30 year long effort to standardize laboratory animals? *Lab. Anim.* **24,** 71–77 (1990).
5. Lehner, B., Crombie, C., Tischler, J., Fortunato, A. & Fraser, A. G. Systematic mapping of genetic interactions in *Caenorhabditis elegans* identifies common modifiers of diverse signaling pathways. *Nature Genet.* **38,** 896–903 (2006).
6. Costanzo, M. *et al.* The genetic landscape of a cell. *Science* **327,** 425–431 (2010).
7. Nowak, M. A., Boerlijst, M. C., Cooke, J. & Smith, J. M. Evolution of genetic redundancy. *Nature* **388,** 167–171 (1997).
8. Rutherford, S. L. & Lindquist, S. Hsp90 as a capacitor for morphological evolution. *Nature* **396,** 336–342 (1998).
9. Queitsch, C., Sangster, T. A. & Lindquist, S. Hsp90 as a capacitor of phenotypic variation. *Nature* **417,** 618–624 (2002).
10. Elowitz, M. B., Levine, A. J., Siggia, E. D. & Swain, P. S. Stochastic gene expression in a single cell. *Science* **297,** 1183–1186 (2002).
11. Wernet, M. F. *et al.* Stochastic spineless expression creates the retinal mosaic for colour vision. *Nature* **440,** 174–180 (2006).
12. Chang, H. H., Hemberg, M., Barahona, M., Ingber, D. E. & Huang, S. Transcriptome-wide noise controls lineage choice in mammalian progenitor cells. *Nature* **453,** 544–547 (2008).
13. Raj, A., Rifkin, S. A., Andersen, E. & van Oudenaarden, A. Variability in gene expression underlies incomplete penetrance. *Nature* **463,** 913–918 (2010).
14. Eldar, A. *et al.* Partial penetrance facilitates developmental evolution in bacteria. *Nature* **460,** 510–514 (2009).
15. Lehner, B. Genes confer similar robustness to environmental, stochastic, and genetic perturbations in yeast. *PLoS ONE* **5,** e9035 (2010).
16. Andachi, Y. *Caenorhabditis elegans* T-box genes *tbx-9* and *tbx-8* are required for formation of hypodermis and body-wall muscle in embryogenesis. *Genes Cells* **9,** 331–344 (2004).
17. Pocock, R., Ahringer, J., Mitsch, M., Maxwell, S. & Woollard, A. A regulatory network of T-box genes and the even-skipped homologue vab-7 controls patterning and morphogenesis in *C. elegans*. *Development* **131,** 2373–2385 (2004).
18. Baugh, L. R. *et al.* Synthetic lethal analysis of *Caenorhabditis elegans* posterior embryonic patterning genes identifies conserved genetic interactions. *Genome Biol.* **6,** R45 (2005).
19. Kafri, R., Bar-Even, A. & Pilpel, Y. Transcription control reprogramming in genetic backup circuits. *Nature Genet.* **37,** 295–299 (2005).
20. DeLuna, A., Springer, M., Kirschner, M. W. & Kishony, R. Need-based up-regulation of protein levels in response to deletion of their duplicate genes. *PLoS Biol.* **8,** e1000347 (2010).
21. Koh, K. & Rothman, J. H. ELT-5 and ELT-6 are required continuously to regulate epidermal seam cell differentiation and cell fusion in *C. elegans*. *Development* **128,** 2867–2880 (2001).
22. Bateson, W. *Mendel's Principles of Heredity* (Cambridge Univ. Press, 1909).
23. Ow, M. C. *et al.* The FLYWCH transcription factors FLH-1, FLH-2, and FLH-3 repress embryonic expression of microRNA genes in *C. elegans*. *Genes Dev.* **22,** 2520–2534 (2008).
24. Vavouri, T., Semple, J. I. & Lehner, B. Widespread conservation of genetic redundancy during a billion years of eukaryotic evolution. *Trends Genet.* **24,** 485–488 (2008).
25. Tischler, J., Lehner, B., Chen, N. & Fraser, A. G. Combinatorial RNA interference in *Caenorhabditis elegans* reveals that redundancy between gene duplicates can be maintained for more than 80 million years of evolution. *Genome Biol.* **7,** R69 (2006).
26. Lehner, B. Conflict between noise and plasticity in yeast. *PLoS Genet.* **6,** e1001185 (2010).
27. Waddington, C. H. Canalization of development and the inheritance of acquired characters. *Nature* **150,** 563–565 (1942).
28. Bobula, J. *et al.* Why molecular chaperones buffer mutational damage: a case study with a yeast Hsp40/70 system. *Genetics* **174,** 937–944 (2006).
29. Van Dyk, T. K. G. A. LaRossa RA. Demonstration by genetic suppression of interaction of GroE products with many proteins. *Nature* **342,** 451–453 (1989).
30. Tokuriki, N. & Tawfik, D. S. Chaperonin overexpression promotes genetic variation and enzyme evolution. *Nature* **459,** 668–673 (2009).

Supplementary Information is linked to the online version of the paper at www.nature.com/nature.

Acknowledgements This work was funded by grants from the European Research Council, Institució Catalana de Recerca i Estudis Avançats, Ministerio de Ciencia e Innovación Plan Nacional BFU2008-00365, Agència de Gestió d'juts Universitaris i de Recerca, ERASysBio+, the European Molecular Biology Organization Young Investigator Programme, the EMBL-CRG Systems Biology Program, by a Formación de Personal Investigador–Ministerio de Ciencia e Innovación fellowship to A.B. and by a Beatriu de Pinós Fellowship to M.O.C. We thank I. Hope, V. Ambros and S. Kim for providing strains. Additional strains were obtained from the Caenorhabditis Genetics Center, which is funded by the National Institutes of Health National Center for Research Resources. We thank T. Zimmermann and R. García from the CRG Advanced Light Microscopy Unit for advice and assistance, J. Miwa and Y. Yamaguchi for 608F antibody, J. Semple for providing complementary DNA clones, A. Marchetti and R. García-Verdugo for technical assistance, J. Tischler and C. Kiel for advice on single-molecule fluorescence *in situ* hybridization and western blotting, respectively, and L. Serrano, M. Isalan and J. Semple for comments on the manuscript.

Author Contributions A.B. performed all experiments, developed the method and analysed the data; M.O.C. demonstrated that increased chaperone activity can suppress mutation outcome in *C. elegans*; A.B. and B.L. designed experiments, conceived the model and wrote the manuscript.

Author Information Reprints and permissions information is available at www.nature.com/reprints. The authors declare no competing financial interests. Readers are welcome to comment on the online version of this article at www.nature.com/nature. Correspondence and requests for materials should be addressed to B.L. (ben.lehner@crg.eu).

METHODS

Expression profiling: image acquisition. Synchronous populations of *tbx-9*(*ok2473*) animals were obtained by treating worms with sodium hypochlorite and then allowing embryos to develop at 25 °C. For a typical time-lapse, around 30–50 gravid worms were picked and then washed three times with M9 buffer in a watch glass. Worms were then transferred to a 50 mm glass-bottomed culture dish (MatTek Corporation). Adults were dissected and released embryos were manually sorted. In a period of time not exceeding 15 min, 4- to 12-cell-stage embryos were collected and carefully placed with an eyelash-pick into the centre of the dish; the rest of embryos and debris were removed using a pipette. A cover slip was placed on top of the worms and sealed with paraffin. Fluorescence and bright-field images in multiple positions were acquired with a ×10 Plan-NEOFLUAR 0.3 NA objective on a Zeiss Cell Observer HS system consisting of an inverted microscope (AxioObserver.Z1) equipped with an automated stage, a C9100-13 IMAG-EM Dual Mode EM-CCD camera (Hamamatsu) and a Sutter DG-4 fast switching xenon light source (Sutter Instrument Company). Temperature control was achieved using a custom microscope incubator box and temperature control device developed by the European Molecular Biology Laboratory (http://www.embl-em.de) coupled to a Unichiller cooling unit (Huber Kältemaschinenbau) for temperature control below room temperature.

At the start of imaging, approximately 25–30 min had elapsed since the dissection of worms. During the first 20 min of the time-lapse no fluorescence illumination was applied, to avoid phototoxicity as early embryos are very sensitive to illumination. Subsequently bright-field and fluorescence images were obtained every 10 min for 8 h, followed by just bright-field images collected every 2 min for 4 more hours or until most of the worms had hatched. The increase in bright-field frequency facilitated the phenotypic score of hatching worms. Exposure times and frequency were adjusted to maximize the signal-to-noise ratio while avoiding phototoxicity (evaluated as approximately 100% hatching of WT (N2) embryos).

The imaging conditions for the *daf-21*, *let-858*, *elt-5* and *flh-2* reporters in a *tbx-9* mutant background were exactly the same as for the *tbx-8* reporter. In the other genetic backgrounds exposure times and acquisition characteristics were adjusted according to the characteristics of the reporter construct. The *tbx-9* reporter was expressed earlier than the *tbx-8* reporter and at lower levels, and the exposure time was increased 2.5× to compensate for this, while reducing the frequency of acquisition to once every 25 min. *The flh-2* reporter was also expressed at lower levels, but the induction was later in development. For this reporter the exposure time was increased (2.5× compared with that for the *tbx-8* reporter), fluorescence acquisition was initiated 1 h later than bright field, but images were still obtained once every 10 min.

When comparing the expression of a particular reporter in two different genetic backgrounds, embryo isolation was performed in 10 min, one strain immediately after the other (total time of 20 min), and image acquisition was performed simultaneously using the conditions previously established for each strain.

Expression profiling: quantification of gene expression. Total fluorescence from each embryo was quantified using ImageJ[31] (http://rsb.info.nih.gov/ij/). First, we performed a global background correction of all images by subtracting an image taken in a region of no fluorescence for each time point. For the *pelt-5::mCherry* reporter data set, an additional flat field correction step was necessary. Background-subtracted images were divided by the homogeneous fluorescence reference to correct for non-homogeneous illumination, and the resulting images used for quantification[32]. The homogeneous fluorescent reference was created by imaging a drop of 0.05 mg ml^{-1} Nile Red solution in M9 buffer. All embryos were visually identified and tagged so that no embryo was counted twice. A region of interest (ROI) was manually drawn around each embryo and an equally sized ROI drawn in the background vicinity; finally, the total fluorescence from each embryo was calculated as the integrated density difference between the embryo containing ROI and the local background ROI. For the particular case of the *flh-2* reporter, at the 100-cell stage most of the reporter signal came from a very restricted area of the embryo. Because embryo background fluorescence was masking this specific source of expression, we quantified it by first drawing an equally sized circle-shaped ROI in all embryos around the signal source and measuring the integrated density. This quantified expression was used for *flh-1* phenotypic prediction.

All embryos were staged using three developmental landmarks: (1) number of cells at beginning of time-lapse, (2) elapsed time until comma stage and (3) elapsed time until twofold-stage. Only those embryos starting the time-lapse at the approximately 6- to 15-cell stage and reaching the next development landmarks with a delay of less than or equal to 30 min were considered for further analysis. In a typical time-lapse, around 10–15 embryos fulfilled those requirements. Data for each reporter–mutant pair prediction included embryos from at least four independent experiments. To correct for day-to-day technical variation (Supplementary Fig. 18), the expression of each embryo was normalized using the mean expression of the population (or populations when comparing the expression of different genotypes) for each time-lapse. For visualization, five time-point smoothing was used for 10 min acquisition frequency recordings, and three time-point smoothing used when the frequency was 25 min.

Data analysis, statistics and figures were generated using R (http://www.r-project.org). Receiver operating characteristic curves for dual reporter predictions were constructed using the ROCR package[33]. Expression levels of *tbx-8* and *daf-21* at comma stage were normalized by subtracting the mean and dividing by the standard deviation of each population. The sum of the normalized values for each embryo was used to calculate the receiver operating characteristic curve of the joint contribution.

Phenotypes. The phenotype of each embryo was scored as WT or abnormal by visual inspection of the hatching morphology. Any abnormal morphology was defined as non-WT. To study the prediction of mutation expressivity, *tbx-9*(*ok2473*) *animals* that hatched with an abnormal phenotype were further classified into two classes. 'Mild' abnormality indicated individuals with a characteristic posterior depression but that conserve the general body structure. 'Severe' embryos were those with severe malformations along most of the posterior axis or the entire body (Supplementary Fig. 19).

Nematode strains and growth conditions. Worms were grown at 20 °C on NGM plates using *Escherichia coli* OP50 as a food source unless otherwise noted. The strains used in and constructed for this study are listed in Supplementary Table 2. Wild type was Bristol N2 (ref. 34). Reporter strains *ptbx-8::GFP* (UL2520) and *pelt-5::GFP* (SD1434) were provided by I. Hope and S. Kim, respectively. The strain VT1343 (*flh-1*(*bc374*)) was a gift from V. Ambros. Some deletion mutations used in this work were provided by the *C. elegans* Gene Knockout Consortium.

We optimized worm growth and embryo imaging conditions for each mutant, to obtain a penetrance with a reasonable representation of embryos hatching with both WT and morphologically abnormal phenotypes. The *tbx-9*(*ok2473*) mutants were maintained at 25 °C and embryos were allowed to develop at 27.5 °C to give a penetrance of approximately 50%; *tbx-8*(*ok656*) were grown at 16 °C and embryos allowed to develop at 20 °C; *flh-1*(*bc374*) mutants were grown at 20 °C and embryos allowed to develop at 26 °C. For *flh-2*(*bc375*) mutants, a growth condition was not found where the penetrance was high enough to be usefully studied.

Reporter gene constructs. We generated transcriptional reporters for the genes *tbx-9*, *flh-2* and *daf-21*. Promoter regions of these genes were amplified from N2 genomic DNA by PCR using the following primer pairs: FW-ptbx-9, 5′-TTGGGTTCAGATAACAATTTGG-3′; RV-ptbx-9, 5′-ATTTTTTGTCTGAAAACGTTAAAATA-3′; FW-pflh-2, 5′-GCGCTTCTCGTGGGCTCT-3′; RV-pflh-2, 5′-ATACAGGCGGTCTGAAAA-3′; FW-pdaf-21, 5′-CGAAACGGTCGAATTTCATAA-3′; RV-pdaf-21, 5′-ATGGTTCTGGAAAAATATCAATTA-3′. The lengths of the amplified regions were 1.5 kb, 1.5 kb and 1.9 kb, respectively. The promoters were cloned into the MultiSite Gateway Entry vector pENTR 5′-TOPO following the manufacturer's instructions (Invitrogen) and then transferred by three-fragment MultiSite Gateway Pro LR reaction (Invitrogen) into the pCFJ150-pDESTttTi5605[R4-R3] destination vector. Middle Entry vectors used were pENTRwGFP or pENTRmCherry; 3′ Entry vector was pCM5.37 containing the *unc-54* 3′ untranslated region (UTR). Final constructs were confirmed by PCR amplification and sequencing.

Strain construction. Strains carrying an extrachromosomal array expressing *ptbx-8::TBX-8::unc-54* 3′ UTR or *ptbx-9::TBX-9::unc-54* 3′ UTR were generated by microinjection as previously described[35] using *pmyo-2::mCherry* as a co-injection marker. The transcriptional reporter *ptbx-9::GFP* was generated by microinjection using *pmyo-2::mCherry* as a co-injection marker, followed by integration using the ultraviolet irradiation method[36]. The transcriptional reporters *pdaf-21::mCherry*, *pdaf-21::GFP*, *phsp-4::mCherry*, *ptbx-8::mCherry* and *pflh-2::GFP* were generated by bombardment in an *unc-119*(*ed3*) background[37,38]. All transgenic strains were backcrossed at least four times. No transgenic strains displayed abnormal phenotypes.

Quantitative PCR. Worms carrying the *pdaf-21*::mCherry transgene were synchronized by hypochlorite treatment, plated as L1 larvae and allowed to develop for 24 h at 25 °C. Larvae were then sorted by hand using a MVX10 Macro Zoom fluorescence microscope (Olympus) into 'high' and 'low' groups based on their mCherry fluorescence levels. Each group had approximately 20 larvae and sorting was performed in triplicate. Worms were washed in M9 and transferred to 1.5 ml Eppendorf tubes containing 200 µl of lysis Buffer (50 mM KCl, 10 mM Tris-HCl (pH 8), 2.5 nM $MgCl_2$, 0.45% Nonidet P-40, 0.45% Tween20) supplemented with 20 µg proteinase K and 20 µg RNase A. Tubes were frozen in liquid nitrogen, followed by incubation at 65 °C for 1 h and 95 °C for 30 min. Genomic DNA was extracted by adding 500 µl Phenol:Chloroform:Isoamyl Alcohol 25:24:1 (Sigma) and precipitated using 600 µl of ice cold ethanol and 50 µl of 3 M NaAc. Quantitative PCR was performed on a LightCycler 480 machine with SYBR green detection (Roche). The transgene was amplified with primers targeting the mCherry coding region: FW-mCherry, 5′-CTACGACGCTGAGGTCAAGA-3′; RV-mCherrry, 5′-CGATGGTGTAGTCCTCGTTG-3′. Transgene levels were normalized by the mean level of two other loci in the genome using

the following primers: FW-daf-21ORF, 5′-TCCAATGACTGGGAAGATCA-3′; RV-daf-21ORF, 5′-CGAACGTAGAGCTTGATGGA-3′; FW-csq-1, 5′-AACTG AGGTTCTGACCGAGAAG-3′; RW-csq-1, 5′-TACTGGTCAAGCTCTGAGT CGTC-3′.

Western blotting. To test whether expression of the *pdaf-21::mCherry* predicted differences in the levels of DAF-21 protein expressed from the endogenous gene, *pdaf-21::mCherry; glp-1*(*e2141*) animals were synchronized as L1 larvae by hypochlorite treatment and starvation at 20 °C overnight. Worms were transferred to plates and allowed to develop for 24 h at 25 °C (*glp-1*(*e2141*) mutation restrictive temperature; this mutation prevents the development of the germ line; *the pdaf-21::mCherry* reporter does not express in germline cells). Larvae were then sorted using an MVX10 Macro Zoom fluorescence microscope (Olympus) into 'high' and 'low' groups based on their mCherry fluorescence. Each group had approximately 30 larvae and sorting was performed in triplicate. Worms were washed in M9 buffer, frozen in liquid nitrogen, dissolved in 30 µl of SDS loading buffer, sonicated for 5 min at 4 °C and then boiled at 95 °C for 5 min. Samples were loaded into a 12.5% SDS polyacrylamide gel and transferred to a nitrocellulose membrane. Primary antibodies were incubated overnight at 4 °C. The following antibodies and dilutions were used: rabbit polyclonal anti-β-actin (ab8227) (Abcam) 1:1,000; rabbit polyclonal anti-DsRed (ClonTech) 1:1,000; mouse monoclonal anti-DAF-21 608F hybridoma supernatant[39] (a gift from J. Miwa and Y. Yamaguchi) 1:40; anti-rabbit IgG peroxidase conjugate (Jackson ImmunoResearch) 1:40,000 and anti-mouse IgG peroxidase conjugate (Sigma-Aldrich) 1:8,000. Quantification of DAF-21 levels in N2 WT and *daf-21*(+/−) was performed in a similar fashion; 30 L4 larvae of each genotype were picked in triplicate. We detected peroxidase activity with SuperSignal West Femto Substrate (Thermo Scientific) and blot imaging was performed using a Fujifilm LAS-3000 luminescent image analyser with exposures times in the lineal range of detection. Finally, band intensities were quantified using ImageJ.

Single molecule fluorescence *in situ* hybridization. We followed the protocol of Raj *et al.*[40] with the following modifications. Probes against *tbx-8* mRNA were generated with the online tool available at www.singlemoleculefish.com and synthesized by Biosearch Technologies. Probes were coupled to CAL Fluor Red 590 fluorophore. The formamide concentration in hybridization and wash buffer was 20% and the total concentration of pooled probes was 25 nM. Hybridization was performed overnight at 30 °C. We imaged embryos using an oil immersion ×100 objective on a Leica DMI4000 inverted microscope equipped with an Evolve 512 EMCCD camera (Photometrics) and a Lumen 200 metal arc lamp (Prior Scientific). We collected stacks of typically 25 images spaced by 0.3 µm for each embryo. Stacks were processed applying a Laplacian of Gaussian filter with the LoG3D plugin[41] for ImageJ. Then dimensionality was reduced by applying a Z-maximum intensity projection (the final image contains the maximum value over all images in the stack at the particular pixel location), and a single threshold was applied to each embryo by visual inspection as recommended. The total number of particles was counted with the 'Analyze particles' ImageJ tool. Embryos were staged by counting the total number of nuclei stained with 4′,6-diamidino-2-phenylindole (DAPI).

Rescue experiments. Worms mutant for *tbx-9* were crossed with a line carrying an extrachromosomal array overexpressing TBX-8 protein and a *pmyo-2::mCherry* reporter as a marker. Adult gravid worms growing at 25 °C were manually sorted under an MVX10 Macro Zoom fluorescence microscope (Olympus) into two groups, one carrying the fluorescent marker, the other lacking it. This latter group served as an internal negative control. Extrachromosomal array transmission was around approximately 50%, meaning that not all embryos in the overexpression group actually carried the transgene, so rescue scores are probably an underestimation. Four- to 12-cell stage embryos were collected in 50 mm glass-bottomed dishes following the same protocol as for time-lapses, and incubated at 27.5 °C. Phenotypes of worms were scored 15 h later. In the case of *tbx-8* mutation rescue, worms were grown at 16 °C and incubated at 20 °C. Control experiments were performed crossing the *tbx-9*(*ok2473*) and *tbx-8*(*ok656*) mutations to a strain carrying the extrachromosomal array *wwEx26*[*pmir-42-44::GFP+unc-119*(+)]. This transcriptional reporter is expressed at high levels during early and late development, and its transmission is approximately 95%. Rescue experiments were performed at least in triplicate for each pair. Finally, repeats were pooled and significance was tested using Fisher's exact test.

31. Abramoff, M. D., Magelhaes, P. J. & Ram, S. J. Image processing with ImageJ. *Biophoton. Int.* **11,** 36–42 (2004).
32. Wolf, D. E., Samarasekera, C. & Swedlow, J. R. Quantitative analysis of digital microscope images. *Methods Cell Biol.* **81,** 365–396 (2007).
33. Sing, T., Sander, O., Beerenwinkel, N. & Lengauer, T. ROCR: visualizing classifier performance in R. *Bioinformatics* **21,** 3940–3941 (2005).
34. Brenner, S. The genetics of *Caenorhabditis elegans*. *Genetics* **77,** 71–94 (1974).
35. Kelly, W. G., Xu, S., Montgomery, M. K. & Fire, A. Distinct requirements for somatic and germline expression of a generally expressed *Caernorhabditis elegans* gene. *Genetics* **146,** 227–238 (1997).
36. Mitani, S. Genetic regulation of mec-3 gene expression implicated in the specification of the mechanosensory neuron cell types in *Caenorhabditis elegans*. *Dev. Growth Differ.* **37,** 551–557 (2003).
37. Praitis, V., Casey, E., Collar, D. & Austin, J. Creation of low-copy integrated transgenic lines in *Caenorhabditis elegans*. *Genetics* **157,** 1217–1226 (2001).
38. Wilm, T., Demel, P., Koop, H. U., Schnabel, H. & Schnabel, R. Ballistic transformation of *Caenorhabditis elegans*. *Gene* **229,** 31–35 (1999).
39. Yamaguchi, Y., Murakami, K., Furusawa, M. & Miwa, J. Germline-specific antigens identified by monoclonal antibodies in the nematode *Caenorhabditis elegans*. *Dev. Growth Differ.* **25,** 121–131 (1983).
40. Raj, A., van den Bogaard, P., Rifkin, S. A., van Oudenaarden, A. & Tyagi, S. Imaging individual mRNA molecules using multiple singly labeled probes. *Nature Methods* **5,** 877–879 (2008).
41. Sage, D., Neumann, F. R., Hediger, F., Gasser, S. M. & Unser, M. Automatic tracking of individual fluorescence particles: application to the study of chromosome dynamics. *IEEE Trans. Image Process.* **14,** 1372–1383 (2005).